IOP Publishing Plasma Physics and Controlled Fusion
Plasma Phys. Control. Fusion 62 (2020) 055014 (8pp) https://doi.org/10.1088/1361-6587/ab7d49

Evolution of electron current layer during anti-parallel magnetic reconnection

Can Huang[1,2], **Aimin Du**[1,2] **and Yasong S Ge**[1,2]

[1] Key Laboratory of Earth and Planetary Physics, Institute of Geology and Geophysics, CAS, People's Republic of China
[2] Innovation Academy for Earth Science, CAS, People's Republic of China

E-mail: huangcan@mail.iggcas.ac.cn

Received 7 January 2020, revised 3 March 2020
Accepted for publication 6 March 2020
Published 8 April 2020

Abstract

Electron current layer (ECL) in the diffusion region plays an important role on energy dispassion and generation of a magnetic island during collisionless magnetic reconnection. In this study, kinetic simulations with high-resolution grids are performed to investigate the evolution of ECL during anti-parallel magnetic reconnection. It is found that ECL splits into two sublayers at the electron inertial scale, not long after the triggering of reconnection. The sublayers keep moving away from each other until reconnection rate reaches the maximum. We find the formation reason and maintaining mechanism of these sublayer structures of the ECL. When electrons flow toward the midplane, out-of-plane velocity is increased by the reconnection electric field. The deflection of magnetic field makes the out-of-plane component of velocity partly converted to the z direction. Electron flows pass through the mid-plane with super-Alfvenic speed. When they enter the other side, the increasing magnetic field makes velocity in the z direction gradually converted to the out-of-plane. Slowdown of the flows causes the density accumulation at the two sides of the mid-plane. The redistribution of electrons brings an extra pressure gradient to the ECS region, balancing the electric force and Ampere force.

Keywords: magnetic reconnection, electron current layer, particle simulation

(Some figures may appear in colour only in the online journal)

1. Introduction

During magnetic reconnection, magnetic free energy is suddenly released with topology change of the magnetic field. In the last seventy years, it has attracted an enormous amount of research on solar [1, 2], planetary [3–5] and laboratory plasmas [6–8] and been widely accepted to explain plasma heating and acceleration [9–11].

Hall dynamics is a critical ingredient in collisionless magnetic reconnection in an ion-electron system [12]. At the scale below the ion inertial length, electrons are frozen in magnetic field lines, while ions can move across magnetic field lines [13–16]. At the scale below the electron inertial length, both ions and electrons are decoupled from the magnetic field lines [12, 17, 18]. Within the electron diffusion region around the X line, electrons travel as the meandering motion [19], and are accelerated directly by the out-of-plane electric field, forming the core part of the electron current layer (ECL) [20, 21]. Electrons carry the significant fraction of the current in magnetic diffusion region. With the proceeding of the reconnection, ECL becomes thinner and longer [21, 22]. Further study has revealed that such evolution arises from the imbalance between the Ampere force and electric force acting on the ECL [22]. By performing 2D particle-in-cell (PIC) simulations of anti-parallel reconnection, Daughton *et al* [23] employed open boundary conditions for the outflows and found the length of the ECL extends to tens of ion inertial lengths. The reconnection rate declines during the extension. During the following generation of magnetic islands, which are excited by the tearing instability in ECL, the fast reconnection rate will be resumed. These influences of evolution of ECL on the reconnection rate have also been studied in a large-scale domain with periodic boundary conditions [21, 24]. Under 3D situation, the evolution of ECL is dominated by the formation and interaction of helical magnetic structures known as flux ropes [25]. The extension of

ECL has also been verified by *in situ* observations in the magnetosheath [26] and magnetotail [27]. Secondary island near the X line has also been identified in the magnetotail [28]. It is further found that ECL is composed of the center diffusion region and elongated electron jets, reaching a length tens of ion inertial lengths in anti-parallel reconnection [29, 30]. Hesse *et al* [31] proposed that the electron flow jets in ECL can be formed by the interaction between the electric drifts and the diamagnetic effects through the combination of the pressure gradients and magnetic field gradients. Considering the energy dissipation in the electron's rest frame, a new measurement of the magnetic diffusion region was suggested by Zenitani *et al* [32]. They found the frozen-in condition is mainly violated within ECL, where the most nonideal energy transfer takes place [33].

Above all, ECL in the diffusion region can affect the reconnection rate, and plays an important role on the energy dispassion and the generation of the secondary island during collisionless magnetic reconnection. As the magnetic free energies are stored centrally in the current layer, it is of great significance to study the evolution of ECL during magnetic reconnection. Previous research showed that ECL can be elongated and thinned [21, 22] with the development of the reconnection. And when the magnetic separatrix angle becomes larger, ECL extends along the separatrix layers and becomes bifurcated. In this study, we have employed higher-resolution grids to investigate the evolution of ECL during anti-parallel magnetic reconnection. It is found that ECL can split into two sublayers, not long after the excitation of magnetic reconnection. Before the reconnection rate reaches the maximum, the two sublayers are separated and move away from each other. By diagnosing the electron distributions and trajectories, we find the reason why the ECL split and its maintaining mechanism. In the following sections, we will introduce the simulation model and initial-boundary conditions at first, then exhibit the simulation results. At last, conclusions and discussions will be made.

2. Simulation model

2D PIC codes are used to simulate the process of anti-parallel magnetic reconnection. Simulations start from a Harris current sheet equilibrium with a particle number density $n(z) = n_b + n_0\mathrm{sech}^2(z/\delta)$, where $n_b = 0.1n_0$ represents the background density, and $\delta = 0.5d_i$ is the half-width of the current sheet. Here d_i (d_e) presents the initial ion (electron) inertial length based on n_0. The initial magnetic field is given by $\mathbf{B}(z) = B_0 \tanh(z/\delta)\mathbf{e}_x$, where B_0 is the asymptotical magnetic field around the current sheet. Both ions and electrons are assumed to be Maxwellian distributed, with an initial temperature ratio $T_{i0}/T_{e0} = 5$ and a mass ratio $m_i/m_e = 64$, where the subscript 'i' ('e') stands for ion (electron). The light speed —Alfven speed ratio is set to be $c/v_A = 15$. The electromagnetic fields are defined on the grids and updated by integrating the Maxwell equations with an explicit leapfrog scheme. As individual particles, ions and electrons and pushed by the updated electromagnetic fields [34]. Simulations are performed

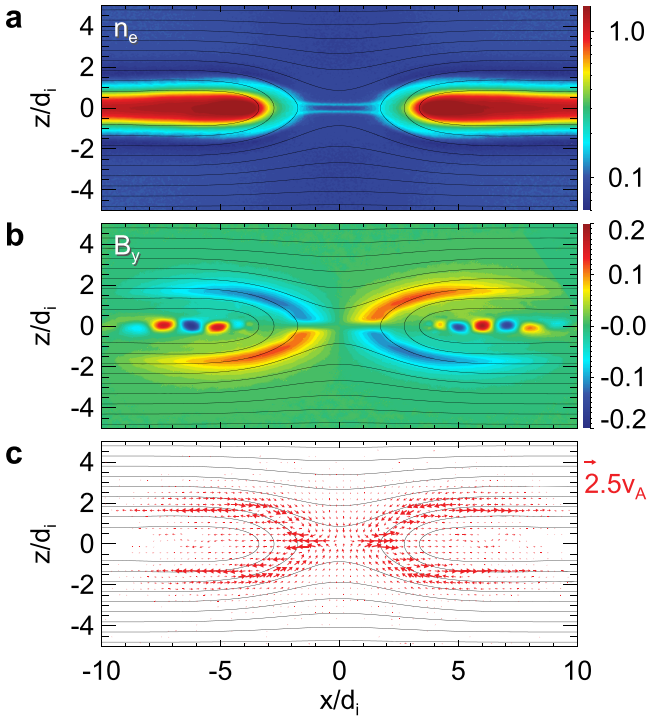

Figure 1. (a) The distributions of electron number density n_e, out-of-plane magnetic field B_y, and electron flow vectors in the entire simulation domain at t = 21 Ω_i^{-1}. The length of the arrow in the right side of figure 1(c) denotes 2.5 v_A. The black contours show the in-plane magnetic field lines.

in the (x, z) plane. Computational domain $[-10d_i, 10d_i] \times [-5d_i, 5d_i]$ and more than 10^8 particles for each species are employed in the simulation. Periodic boundary conditions are assumed in the x direction, while conducting boundary conditions are retained and particles are specularly reflected at the boundaries in the z direction. The reconnection is initiated by a tiny local flux perturbation located at the center of the simulation domain [35]. It is worth noting that high-resolution grids are utilized here. The spatial resolution is $\Delta x = \Delta z = 0.005d_i = 0.04d_e$. The time step is set to be $\Delta t = 0.0002\Omega_i^{-1}$, where $\Omega_i = eB_0/m_i$ is the ion gyrofrequency. These setups can make sure that there are more than 25 data points to capture the electron's behaviors below the electron inertial scale. The ion-electron inertial length ratio $d_i/d_e = 8$ is large enough to distinguish the behaviors of ions and electrons, in view of the limited computing resources.

3. Simulation results

Figure 1 shows the distributions of electron number density, out-of-plane magnetic field, and electron flow vectors in the whole simulation domain at t = 21 Ω_i^{-1}. The magnetic reconnection site is located at the center of the simulation domain. Around the X line, electrons are distributed in two thin layers. As a characteristic of Hall reconnection, a quadruple structure of B_y is shown in figure 1(b). Electrons flow toward the X line along the separatrix, and flow out along the

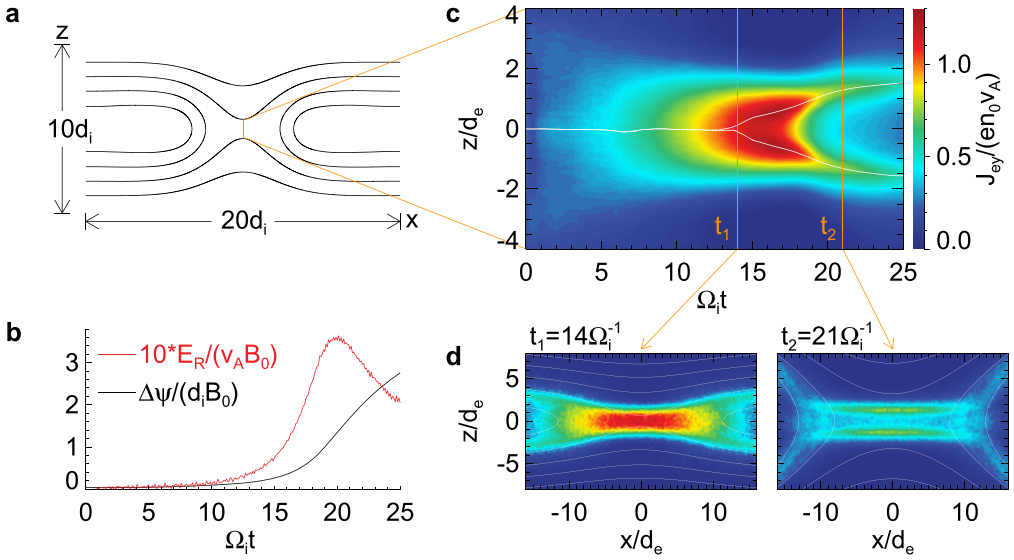

Figure 2. (a) The representative configuration of the magnetic fields during magnetic reconnection in the simulations. (b) The reconnected flux (black) and the reconnection rate (multiplied by ten, red). (c) Time evolution of J_{ey} along $x = 0$. The white lines denote the peaks of the current density. (d) The distributions of J_{ey} at t = 14 Ω_i^{-1} and t = 21 Ω_i^{-1}. The white contours show the in-plane magnetic field lines.

magnetic field lines inside the separatrix, which forms the Hall current system in the diffusion region.

The process of the magnetic reconnection and evolution of ECL are presented in figure 2. Figure 2(a) shows the configuration of the magnetic field lines at a representative time during reconnection. The reconnected flux (the flux difference between the X line and the center of the Harris current sheet) and the reconnection rate are presented with black and red lines in figure 2(b), respectively. Reconnection starts around t = 12 Ω_i^{-1}, and the reconnection rate increases rapidly between t = 15 Ω_i^{-1} and t = 20 Ω_i^{-1}. Then the rate decreases. Magnetic reconnection reaches saturation at t = 30 Ω_i^{-1} in the simulation, which is not shown in figure 2(b). With the development of the reconnection, electrons are accelerated by the out-of-plane electric field in the vicinity of the X line, which forms the ECL [21, 22]. Evolution of the ECL is shown in figure 2(c), which is plotted by extracting the data of electron current density along the orange segment in figure 2(a) at different times. The white lines denote the peaks of the current density. The half width of the ECL narrows into about 2 d_e at t = 14 Ω_i^{-1}, then the ECL splits into two sublayers with a half width of d_e. Then the two sublayers keep moving away from each other. The separation speed reaches about 0.05 v_A at t = 17 Ω_i^{-1}. The separation slows down gradually after t = 20 Ω_i^{-1}, and stops at about t = 24 Ω_i^{-1}. Moreover, the peak current density rises till t = 17 Ω_i^{-1}, then declines. Figure 2(d) gives the distributions of electron current at two representative times. Before t = 14 Ω_i^{-1}, the ECL has only one layer. At t = 21 Ω_i^{-1}, it evolves into two sublayers which are apart from each other about 3 d_e. Comparing figure 2(c) with 2(b), it is clear that the splitting follows the start of magnetic reconnection, and the separation of the sublayers is enhanced between t = 15 Ω_i^{-1} and t = 20 Ω_i^{-1}, when the reconnection is in the rapid-growth phase. The separation slows down and stops when the reconnection rate declines.

Figure 3 exhibits the details of the ECL at t = 21 Ω_i^{-1} when it splits into two sublayers. The profile of J_{ey} along $x = 0$ is plotted in figure 3(a) and the gray line presents the drift current caused by $\mathbf{E} \times \mathbf{B}$. The widths of the sublayers are about d_e, and the current peaks at $z = \pm 1.4 d_e$. In the outer region ($|z| > 3d_e$), the drift current density J_{Dy} is consistent with J_{ey}, which means the motion of the electrons is determined mostly by the electric drift. In other words, electrons are frozen in the magnetic field in the outer region. In the inner region ($|z| < 3d_e$), electrons are decoupled from the magnetic field and accelerated by the reconnection electric field to form the enhanced J_{ey} which exceeds the current density determined by drift motion. It shows a two-scale structure [36] of an intense ECL embed in a broader current layer at ion scales. Figure 3(b) gives the electron distribution f in the phase space (z, v_{ez}) along $x = 0$. There is a hole in the center of the phase space, which is also found in a driven reconnection simulation by Horiuchi and Ohtani [37]. Electrons flow into the vicinity of the X line from the outer region with $v_{ez} = 0.1 v_A$ (estimated from f in the outer region). v_{ez} increases when electrons enter the inner region, and decreases after electrons pass through the mid-plane. Counter-streaming distribution of electrons in the inner region exists, which constitutes the core part of the phase hole. The distribution f in the phase space (z, v_{ey}) along $x = 0$ is plotted in figure 3(c). In the outer region, electrons move with the magnetic field lines. In the inner region, electrons can be accelerated in the y direction to $-(5\text{-}10)v_A$.

The forces acting on a hypothetical electron in the z direction are plotted in figure 3(d). Note that B_y and B_z are almost zero along $x = 0$, therefore the electric force $F_E \sim -eE_z$(red) and the magnetic force (Lorentz force) $F_B \sim ev_{ey}B_x$(green). The total force is denoted by the black

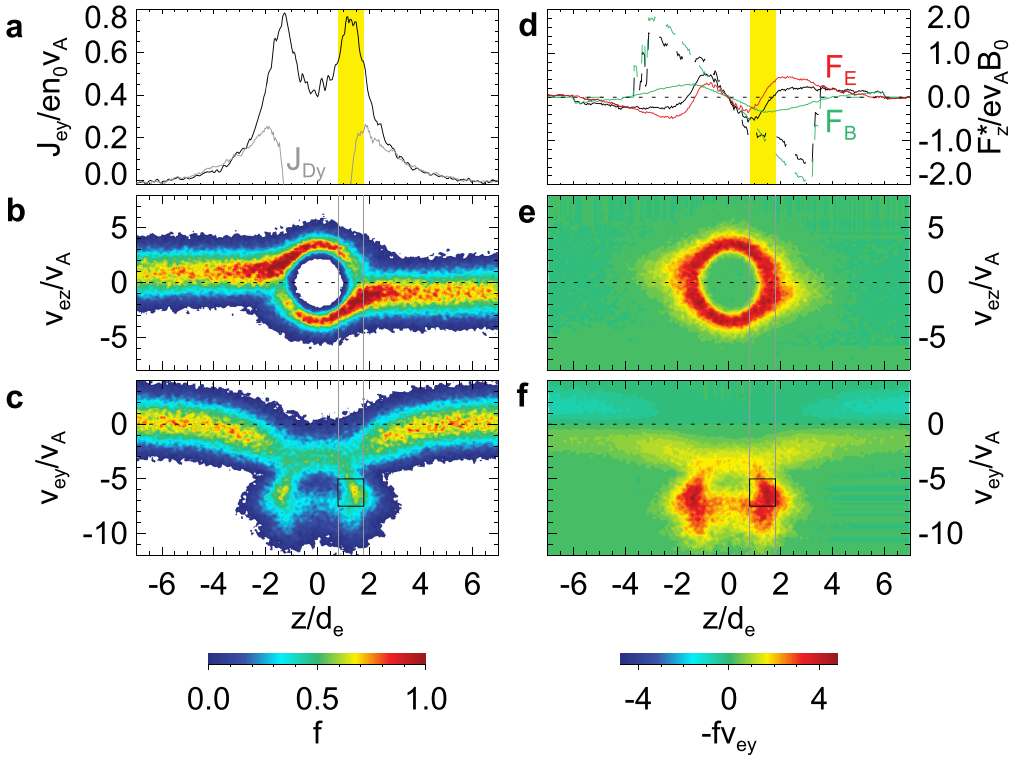

Figure 3. (a) The profile of J_{ey} along $x = 0$ at t = 21 Ω_i^{-1}. The gray line presents the drift current caused by $\mathbf{E} \times \mathbf{B}$. (b) The electron distribution f in the phase space (z, v_{ez}) along $x = 0$. (c) Electron distribution f in the phase space (z, v_{ey}) along $x = 0$. (d) The electric force (red), magnetic force (green), and total force (black) acting on an electron in the z direction. The solid and dashed lines represent the forces calculated from the electrons with $v_{ey} > -5v_A$ and $-10v_A < v_{ey} < -5v_A$ from figure 3(c), respectively. (e) The distributions of $-v_{ey}f(z, v_{ez})$. (f) The distributions of $-v_{ey}f(z, v_{ey})$. The yellow regions in figures 3(a) and (d), as well as the regions between the two gray lines in figures 3(b)–(e), denote the upper sublayer of the ECL.

line. The solid and dashed lines represent the forces calculated from the electrons with $v_{ey} > -5v_A$ and $-10v_A < v_{ey} < -5v_A$ from figure 3(c), respectively. Such classification can help to understand the behavior differences between the electrons with lower and higher v_{ey}. In the inner region, the profile of F_B presents a bipolar structure and it is negative (positive) in the upper (lower) half-space. In the region $|z| < 1.3d_e$, the electric force points to the mid-plane, while it points away from the mid-plane in the region $|z| > 1.3d_e$. The total force points to the mid-plane, which means that electrons can be trapped in the inner region in the z direction. Such trapping can maintain the ECL for a longer time, even if the magnetic reconnection is entering into the saturation stage. For the electrons with lower $v_{ey}(v_{ey} > -5v_A)$, electric force and magnetic force are both significant, while the behaviors of the electrons with higher $v_{ey}(-10v_A < v_{ey} < -5v_A)$ are mainly controlled by magnetic force. It implies that there may be a specific electron acceleration mechanism caused by the existence of sublayers, which will be studied in our future work. A concise method is utilized here to find the electrons which contribute mostly to J_{ey}. We call these electrons 'carriers'. Figures 3(e) and (f) show the distributions of $-v_{ey}f(z, v_{ez})$ and $-v_{ey}f(z, v_{ey})$, respectively. These carriers are mostly located in a ring (roughly located in the region $1 < \sqrt{(z/1.3d_e)^2 + (v_{ez}/3v_A)^2} < 1.5$) in the ($z$, v_{ez}) space, and in the region $|z| < 2d_e$ with $-10 < v_{ey}/v_A < -4$ in the (z, v_{ez}) space. The yellow region in both figures 3(a) and (d) denotes the location of the upper sublayer of ECL. As shown in figures 3(b) and (e), in this sublayer, carriers have two populations: most of them flow into the mid-plane from the upper half-space and a small fraction of them move up from the lower half-space. The carriers are mostly focused in the black box marked in figures 3(c) and (f). In order to understand the dynamic behaviors of the carriers, we have traced the electrons within the black box.

There are tens of thousands of electron carriers traced in the rerun of the simulation. Their behaviors are almost similar. Figure 4(a) gives the trajectory of a typical electron that is located in the black box in figure 3 at t = 21 Ω_i^{-1}. The numbers on the figure denote the simulation times normalized to Ω_i^{-1}, and the red boxes show the approximate position of the two sub current layers. The color-filled contours show the distribution of the total force in the z direction calculated by the average v_{ey} for each z in figure 3(c), and the white lines present the in-plane magnetic field lines. From t = 20 Ω_i^{-1} to t = 20.7 Ω_i^{-1}, the electron drifts toward the ECL region from the lower half-space. It is trapped in the inner region between the interval 20.8 Ω_i^{-1} < t < 21.3 Ω_i^{-1}. The electron gets reflected back in the sublayers twice, then moves toward the x direction and escapes to the flux pile-up region. The electron travels as meandering motion, except the acceleration in the -y direction. Note that the main body of such motion in this

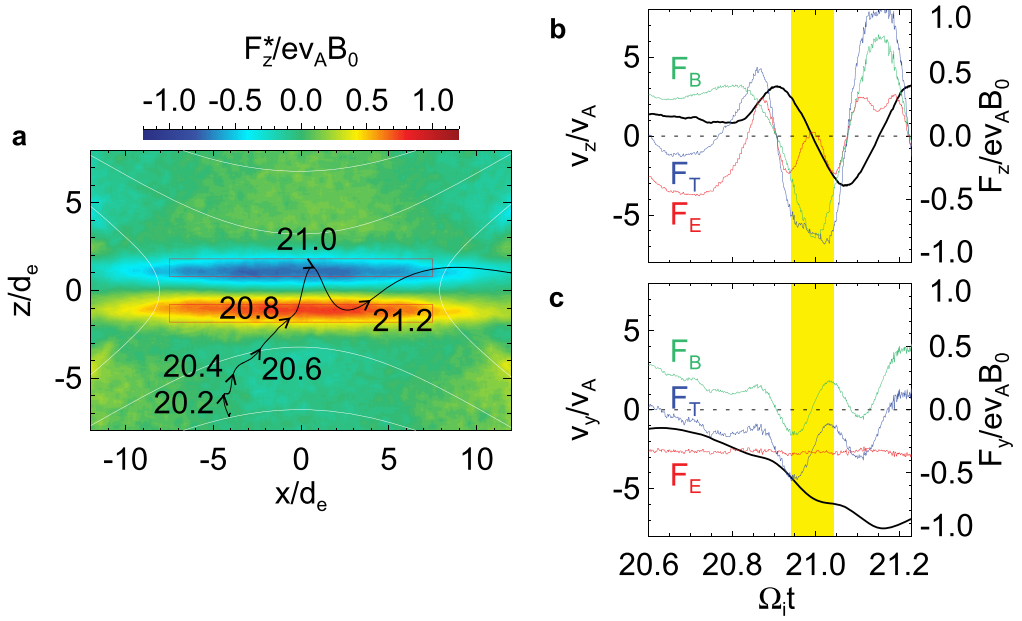

Figure 4. (a) The trajectory of a typical electron that is located in the black box in figure 3. The background colors show the distribution of the total force (calculated by the average v_{ey} for each z in figure 3(c)) in the z direction. (b) Velocity and forces along the trajectory in the z direction. (c) Velocity and forces along the trajectory in the y direction. The thick black lines show the velocities. The red, green and blue lines present the electric, magnetic, and total forces, respectively.

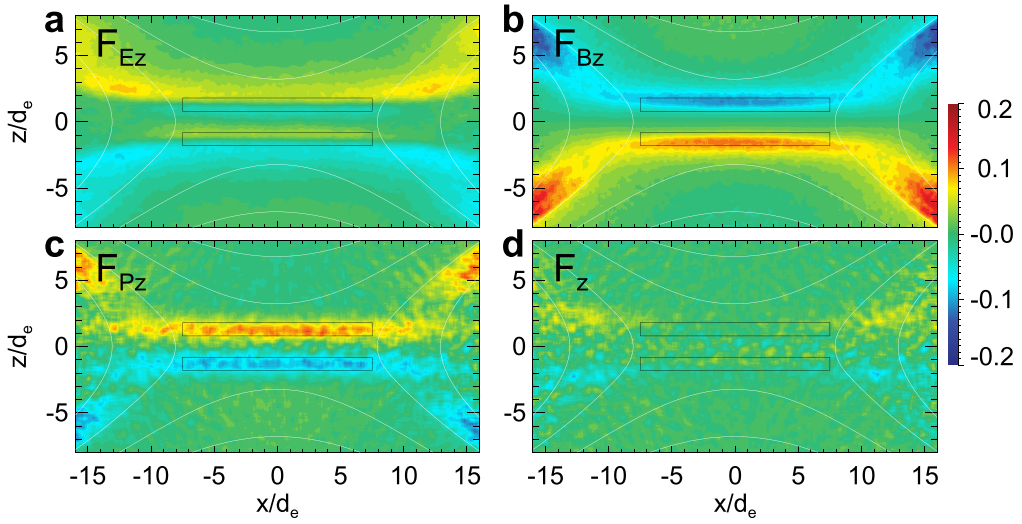

Figure 5. The distributions of (a) electric force $F_{Ez} = -en_eE_z$, (b) Ampere force $F_{Bz} = (\mathbf{J}_e \times \mathbf{B})_z$, (c) electron pressure force $F_{Pz} = (-\nabla \cdot \mathbf{P}_e)_z$, and (d) total force $F_z = F_{Ez} + F_{Bz} + F_{Pz}$ acting on the ECL in the z direction at t = 21 Ω_i^{-1}. The black boxes show the approximate position of the two sub current layers.

simulation is electron flows rather than random particles. Figures 4(b) and (c) give the velocities (thick black lines) and forces along the trajectory. The red, green and blue lines present the electric, magnetic, and total forces, respectively. In the z direction, the electron is reflected twice as shown in figure 4(a), while it keeps accelerating in the -y direction due to the out-of-plane electric field E_y. Focusing attention on the yellow region, during which the electron goes into and gets reflected out from the upper sublayer, we can understand the electron behaviors more clearly. When the electron moves through the mid-plane the first time, v_{ez} reaches the peak. Then it enters into the upper sublayer, and gets decelerated in the z direction by the negative F_E and F_B. At $t \sim 21\Omega_i^{-1}$. v_{ez} turns negative and the electron is reflected toward the lower sublayer.

Figure 5 plots the electric force $F_{Ez} = -en_eE_z$, Ampere force $F_{Bz} = (\mathbf{J}_e \times \mathbf{B})_z$, electron pressure force $F_{Pz} = (-\nabla \cdot \mathbf{P}_e)_z$, and total force $F_z = F_{Ez} + F_{Bz} + F_{Pz}$ acting on the ECL in the z direction at t = 21 Ω_i^{-1}. The black boxes show the approximate position of the two sub current layers. The electric force points from the center line of the sublayer to the upper and lower edges. The magnetic force points to the mid-plane, and it is greater at the outer edge (farther away from the mid-plane) of the sublayer. The

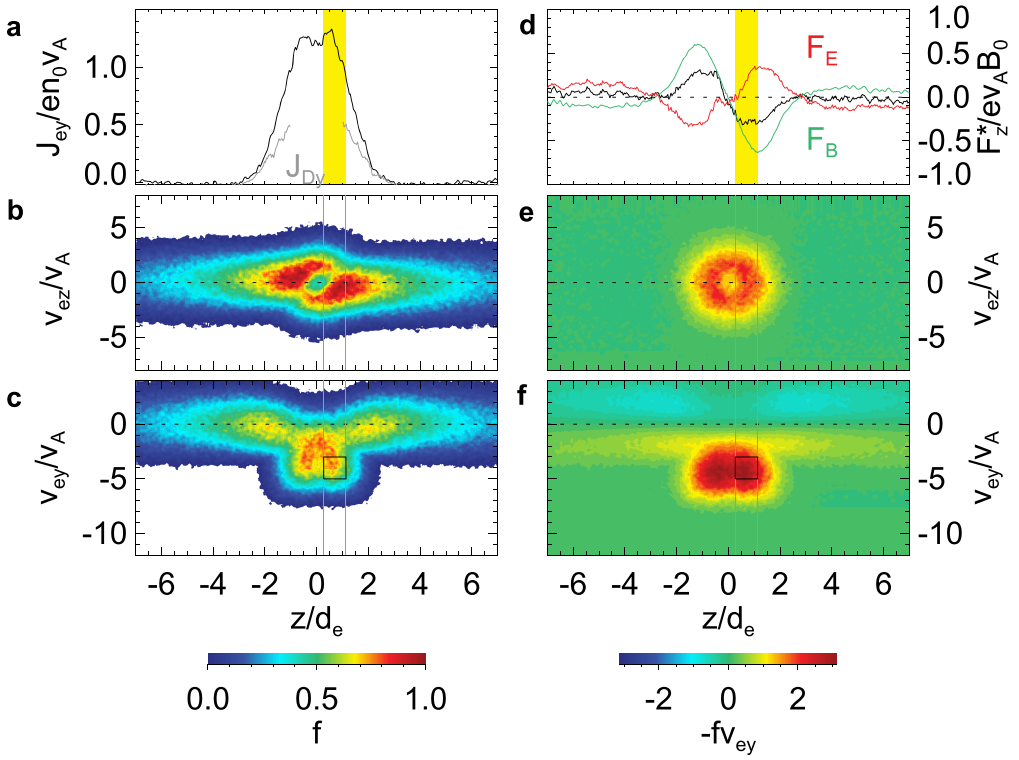

Figure 6. The format is the same as figure 3, except the data is obtained at t = 16 Ω_i^{-1}.

pressure force points away from the mid-plane, and it is larger at the inner edge of the sublayer. The total force is close to zero, which means sublayers are force balanced and quasi-steady. The extra pressure tensor gradient caused by the redistributed electrons balances the electric force and magnetic force.

The results from figures 3–5 demonstrate that the double-sublayer configuration of the ECL can be self-sustained if the split of the ECL is formed and the magnetic reconnection continues. To know the reason why the ECL split happens since the start of the reconnection, the dynamics of the carrier electrons at the earlier stage should be investigated. The form of figure 6 is the same as that of figure 3, except the data is obtained at t = 16 Ω_i^{-1} when it is not long after the split starts. Figure 6(a) shows a less obvious double-peak structure, which indicates that the split occurred not long ago. A smaller phase hole in figure 6(b) means that the electron flows begin to accelerate in the $\pm z$ directions. As shown in figure 6(d), the electric force has a bipolar structure and is always opposite to the magnetic force, which is very different from that at t = 21 Ω_i^{-1}. Nevertheless, the magnetic force is so much stronger that the total force confines electron carriers within the ECL region.

We have also traced the electrons located in the black box marked in figures 6(c) and (f). The trajectory of a typical electron is exhibited in figure 7(a). The electron moves from the left upper-half space to the right during 15.4 Ω_i^{-1} < t < 16.4 Ω_i^{-1}. In the ECL, it is reflected once by the upper sublayer and twice by the lower sublayer. The thick black lines (v_{ez} and v_{ey}) in figures 7(b) and (c) show these reflections in the z direction and the gradual acceleration in the −y direction. The magnetic force and electric force are opposite in the z direction, and the latter is much smaller than the former. When the electron moves toward the ECL region with an increasing $|v_{ey}|$ from upstream, the Lorentz force $ev_{ey}B_x$ becomes stronger. The deflection by the magnetic field B_x leads to that v_{ey} is fractionally transformed to v_{ez}, which causes the increase of v_{ez} when electrons move closer to the ECL. This is the formation mechanism of the phase hole in the space (z, v_{ez}) in the ECL region at the early stage of the magnetic reconnection. In other words, the start of the reconnection excites the out-of-plane electric field, which directly speeds up the partly-magnetized electrons in the -y direction near the mid-plane. Then these electron flows with higher v_{ez}, converted from the accelerated v_{ey}, pass through the mid-plane and reach a farther place than before. When they enter the other side of the mid-plane, the increasing magnetic field makes v_{ez} converted to v_{ey}. At last, the slowdown of the electron flows in the z direction by the magnetic force leads to the accumulation of J_{ey} at the two sides of the mid-plane. A double-peak structure of J_{ey} forms.

4. Conclusions and discussions

In this study, we have performed 2D PIC simulations with high-resolution grids ($\Delta x = 0.04d_e$), which can fully capture electron trajectories during anti-parallel magnetic reconnection. It is found that electron can be accelerated directly in the vicinity of the X line to form the original ECL. About two Ω_i^{-1} s after the start of magnetic reconnection, ECL begins to split into the upper and lower sublayers. As magnetic reconnection advances into the rapid growth stage, the distance between the two sublayers increases. When the reconnection rate reaches the maximum and begins to decline, the

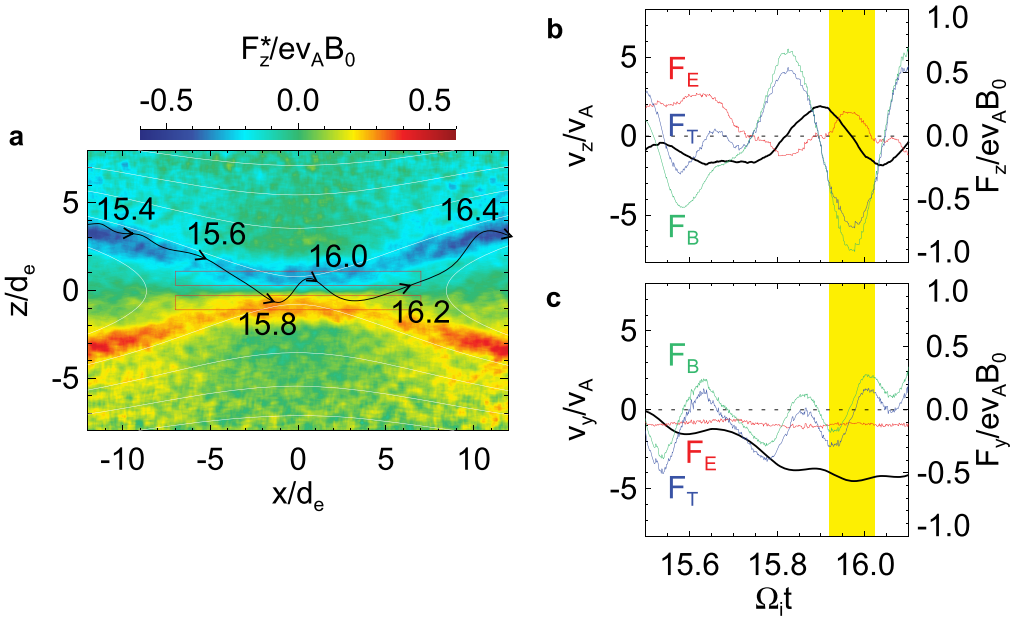

Figure 7. The format is the same as figure 4. The data is collected in the interval 15.4 Ω_i^{-1} < t < 16.4 Ω_i^{-1}.

separation stops and the two sublayers remain quiescent except the current density decreases. Along with the formation of the ECL sublayers, an electron hole appears in the ECL region in the phase space (z, v_{ez}). The most carriers of the current layers are concentrated around the phase hole. In other words, electrons from the upper and lower half-space are trapped in the vicinity of the mid-plane and become the 'stable' carriers of the ECL. By tracing the main body of the carriers, we find the electrons have similar trajectories within the ECL: reflected several times between the two sublayers. Electrons are gradually accelerated in the −y direction by the out-of-plane electric field, while they are trapped within the ECL by the electromagnetic forces in the z direction.

By the combination of the electron behaviors within ECL at t = 14 Ω_i^{-1} and t = 21 Ω_i^{-1}, we find the reason of the split of the ECL and the maintaining mechanism of the two sublayers. In the early stage of reconnection (before the fast growth stage), the out-of-plane electric field E_y starts to be excited. Electrons flow into the vicinity of the X-line from the two sides of the mid-plane, and velocities increase in the -y direction. When they move closer and closer to the mid-plane, the deflection of the magnetic field B_x leads to that v_{ey} is partly converted to v_{ez}. This makes electron flow reach a father place in the z direction. After it rushes through the mid-plane and starts to be coupled with the increasing B_x, the decrease of the bulk velocity in the z direction makes the density accumulation at the two sides of the mid-plane. Thus, the split of the ECL occurs. With the growth of the reconnection rate, electrons reach and get reflected at a position which is farther and farther away from the mid-plane. At the same time, the electron density accumulation also causes the rise of electrostatic field E_z within the ECL region. This electrostatic field points away from the mid-plane and can prevent the separation of the sublayers, which can be confirmed by the force analysis shown in figures 4(b) and 5(a). The higher reconnection rate brings the stronger electron acceleration in the −y direction, which leads to the faster v_{ez} at the mid-plane. This will increase the distances between the two sublayers. But the electron pressure gradient and electrostatic field caused by the electron redistribution can repress this trend. When they reach equilibrium, the separating is suspended. Therefore, the separation stops when the reconnection rate starts to decline.

An extra case is performed with a higher mass ratio $m_i/m_e = 625$, temporal resolution $\Delta t = 5 \times 10^5 \Omega_i^{-1}$ and spatial resolution $\Delta x = 2 \times 10^{-3} d_i = 5 \times 10^{-2} d_e$. In this case, dynamics on electron scale can be completely distinguished from ion scale and hybrid scale of $\sqrt{d_i d_e}$. It is found that the width of the sublayer is about d_e, the same with the case of $m_i/m_e = 64$. The width of the entire ECL (including the two sublayers), or the separation of the two sublayers, is about $6d_e$, which is on a hybrid scale, which is consistent with the results from the experiments. These results of the simulations give us a new image of ECL and associated electron dynamics in the magnetic diffusion region during collisionless magnetic reconnection. Compared to the traditional knowledge about the electron diffusion region, there should be some differences in the energy conversion process and energization of electrons after the generation of the sublayers of ECL. Electrons can be trapped and reflected between the two sublayers many times, which implies that the existence of ECL split may help to generate high energy electron flux in the diffusion region more effectively. Additionally, sublayers are not located in the midplane or at the null point, which means the energy conversion may take place before magnetic field lines arrive the midplane. They are worth studying in our future work.

Acknowledgments

This work is supported by the National Natural Science Foundation of China, grant nos. 41974173, 41674168, Beijing Municipal Science and Technology Commission (grant no. Z191100004319001), and the Strategic Priority Research Program of Chinese Academy of Sciences (grant no. XDA14040404).

ORCID iDs

Can Huang https://orcid.org/0000-0003-0223-0494

References

[1] Giovanelli R G 1946 *Nature* **158** 81–2
[2] Masuda S, Kosugi T, Hara H and Ogawara Y 1994 *Nature* **371** 495–7
[3] Øieroset M, Phan T D, Fujimoto M, Lin R P and Lepping R P 2001 *Nature* **412** 414–7
[4] Zhang T L *et al* 2012 *Science* **336** 567–70
[5] Wang R S, Lu Q M, Huang C and Wang S 2010 *J. Geophys. Res.* **115** A01209
[6] Ji H T, Yamada M, Hsu S and Kulsrud R 1998 *Phys. Rev. Lett.* **80** 3256–9
[7] Li C K, Seguin F H, Frenje J A, Rygg J R, Petrasso R D, Town R P J, Landen O L, Knauer J P and Smalyuk V A 2007 *Phys. Rev. Lett.* **99** 055001
[8] Dong Q L *et al* 2012 *Phys. Rev. Lett.* **108** 215001
[9] Vasyliunas V M 1975 *Rev. Geophys.* **13** 303–36
[10] Biskamp D 2000 *Magnetic Reconnection in Plasmas* (Cambridge: Cambridge University Press)
[11] Priest E and Forbes T 2000 *Magnetic Reconnection: MHD Theory and Applications* (Cambridge: Cambridge University Press)
[12] Birn J *et al* 2001 *J. Geophys. Res.* **106** 3715–9
[13] Sonnerup B U Ö 1979 *Magnetic Field Reconnection, in Solar System Plasma Physics* (New York: North-Holland)
[14] Terasawa T 1983 *Geophys. Res. Lett.* **10** 475–8
[15] Shay M A, Drake J F, Rogers B N and Denton R E 2001 *J. Geophys. Res.* **106** 3759–72
[16] Lu Q M, Huang C, Xie J L, Wang R S, Wu M Y, Vaivads A and Wang S 2010 *J. Geophys. Res.* **115** A11208
[17] Ma Z W and Bhattacharjee A 2001 *J. Geophys. Res.* **106** 3773–82
[18] Pritchett P L 2001 *J. Geophys. Res.* **106** 3783–98
[19] Speiser T 1965 *J. Geophys. Res.* **70** 4219–26
[20] Hoshino M, Mukai T, Terasawa T and Shinohara I 2001 *J. Geophys. Res.* **106** 25979–97
[21] Fujimoto K 2006 *Phys. Plasmas* **13** 072101
[22] Huang C, Lu Q, Yang Z, Wu M, Dong Q and Wang S 2011 *Nonlin. Processes Geophys.* **18** 727–33
[23] Daughton W, Scudder J and Karimabadi H 2006 *Phys. Plasmas* **13** 072101
[24] Daughton W 2007 *Eos Trans. AGU* **88** 23
[25] Daughton W, Roytershteyn V, Karimabadi H, Yin L, Albright B J, Bergen B and Bowers K J 2011 *Nat. Phys.* **7** 539–42
[26] Phan T D, Drake J F, Shay M A, Mozer F S and Eastwood J P 2007 *Phys. Rev. Lett.* **99** 255002
[27] Chen L J *et al* 2008 *J. Geophys. Res.* **113** A12213
[28] Wang R, Lu Q, Du A and Wang S 2010 *Phys. Rev. Lett.* **104** 175003
[29] Karimabadi H, Daughton W and Scudder J 2007 *Geophys. Res. Lett.* **34** L13104
[30] Shay M A, Drake J F and Swisdak M 2007 *Phys. Rev. Lett.* **99** 155002
[31] Hesse M, Zenitani S and Klimas A 2008 *Phys. Plasmas* **15** 112102
[32] Zenitani S, Hesse M, Klimas A and Kuznetsova M 2011 *Phys. Rev. Lett.* **106** 195003
[33] Zenitani S and Umeda T 2014 *Phys. Plasmas* **21** 034503
[34] Birdsall C K and Langdon A B 1991 *Plasma Physics via Computer Simulation* (New York: McGraw-Hill)
[35] Huang C, Lu Q M, Guo F, Wu M Y, Du A M and Wang S 2015 *Geophys. Res. Lett.* **42** 7282–6
[36] Ishizawa A, Horiuchi R and Ohtani H 2004 *Phys. Plasmas* **11** 3579–85
[37] Horiuchi R and Ohtani H 2008 *Commun. Computational Phys.* **4** 496–505